

# CHARACTERIZATION AND MODELING OF A THERMAL CONDUCTIVITY SENSOR FOR LIQUIDS

*Job Harbers*

## Abstract

Accurate thermal conductivity measurements are difficult to achieve and require intricate and costly devices. Microfluidic solutions could aid in cutting down on costs while improving speed and efficiency due to the microscale test volume. In this paper, we aim to characterize a micromachined thermal conductivity sensor. We start by modeling the sensor to validate the design. Simultaneously, the model provides insight into the effects that relevant sensor parameters have on the thermal conductivity readings. Next, we perform measurements that validate the findings obtained through simulation. Lastly, measurements of liquids with distinct thermal conductivity are carried out to find a characterization coefficient. This coefficient facilitates the conversion of the sensor output into the measured thermal conductivity. We conclude that the sensor shows promising results, with a full-scale deviation of as low as 2%. However, further research is required to pinpoint the cause for inconsistent readings that prevent commercial viability.

## INTRODUCTION

Fluid characterization is an integral part of certain industries, as many manufacturers use certain mixtures of liquids to fabricate their products. These include mixtures like chemicals and medicinal goods where the exact composition of said substance is of great importance. Traditional labs can characterize these fabricated batches to ensure their quality. However, the amount of volume needed for testing can be quite substantial when dealing with more expensive and rare fluids. The use of microfluidic sensors can help to greatly reduce the needed testing volume [1]. Furthermore, it can help cut down on needed personnel if it is implemented with an intuitive and smart characterization interface combined with automation capabilities. A series of microfluidic sensors on a single chip can even help reduce the needed volume further [2]. A fluid has several characteristics that can be used to obtain its composition, e.g. volumetric heat capacity, viscosity, electric permittivity, density, and thermal conductivity. Accurately ascertaining enough of these characteristics eventually narrows down the list of possible fluid compositions, making identification possible. In this paper, we characterize one of these sensors, a thermal conductivity sensor (TCD). The following section is dedicated to the architecture and design of the sensor in order to visualize the working principle of the sensor. Secondly, the sensor is analyzed and modeled. Lastly, the empirical data that aided in the characterization of the sensor is presented and discussed.

## SENSOR DESIGN

The working principle of the sensor resides in the amount of heat transfer between the thermally isolated heater and the relatively large silicon substrate. The conduction is governed by the thermal conduction through the fluid that resides in the channel. According to Fourier's law of steady-state thermal conduction, the fluid acts as a thermal resistance proportional to the reciprocal of its thermal conductivity. When heat is applied, thermal resistance induces a temperature difference between the two entities that it separates. In this instance, a volumetric heat flux is generated in the heater by means of DC current excitation. The induced temperature difference ( $\Delta T$ ) is linearly dependent on the size of the thermal resistance. When a metal is heated, its electrical resistivity is altered and can be calculated from:

$$R = \frac{\rho_0(1 + \alpha\theta \cdot l)}{A} \quad (1)$$

Each metal has a thermal coefficient of resistance (TCR) which dictates the influence of temperature on its electrical resistivity. Platinum has a fairly linear TCR ( $\alpha$ ) for moderate temperature changes [3], this makes it suitable to use as a temperature sensor as one can calculate the temperature rise based on the rise in electrical resistance. This is the reason that the sensor employs a platinum readout track that is sputtered on top of the channel. The fabrication process follows the general procedure described in [2]. In figure 1 we can find the architecture of the sensor to be analyzed. There are walls surrounding the channel, these are constructed by filling etched trenches with silicon-rich silicon nitride (SiRN). SiRN has properties favorable to highly doped silicon, it electrically isolates the readout and heater from the bulk and fluid. Furthermore, the SiRN walls together with the physical separation from the bulk at the sides of the channel allow for better thermal isolation. This thermal isolation provides higher resolution due to the fact that the conduction through the working fluid becomes the path of least resistance. Any changes in its magnitude have significant consequences for the temperature rise as a result, thus enhancing the sensitivity of the sensor. The exact dimensions associated with the channel can be found in table 1.

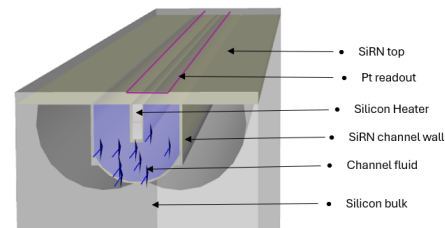


Figure 1: Layout of the thermal conductivity sensor

Table 1: Dimensions concerning the sensor

Physical entity	Dimensions [um]
Wafer thickness	525
SiRN wall thickness	1.0-2.5
Channel length	1000
Channel width	63.6
Channel height	60
Heater height	40
Heater width	9
Pt readout track width	4

## ANALYSIS AND MODELING

### CIRCUIT ANALOGY

The thermal behavior of the heat flow from the heater to its surroundings is analogous to that of the electrical domain. Heat flow is analogous to a current source, the thermal resistances can be modeled as such, while the surrounding ambient temperature of the air resembles ground. There are three resistances that together make up the model. The thermal resistance of the heat transferred through the channel by conduction through the liquid, heat conduction through the channel walls, and the heat convection from the substrate to the surrounding air. Firstly, we approximate the resistance through the fluid ( $R_{th,f}$ ). The channel remains attached to the substrate on its underside. However, the surface area of this contact is unknown due to the uncertainty in the fabrication process. The most fitting geometry is a semi-cylindrical one, where the underside edge of the heater is the inner surface, and the contact with the bulk is the outer surface. We start off by taking Fourier's law applied to a cylindrical geometry [4] while keeping in mind the expression for thermal resistance:

$$q = -\kappa A \frac{dT}{dr} \quad \Delta T = q \cdot R_{th,f} \quad (2)$$

The equation is rearranged to have all terms concerning radii on the left side, after which both sides are integrated to lose  $dr$  and  $dT$  respectively. Note that the surface area  $A$  is half that of an open ended cylinder which equates to  $\pi rL$ .

$$\int_{r_1}^{r_2} \frac{q}{A} dr = \int_{T_1}^{T_2} -\kappa dT \quad (3)$$

Working these integrals out and rearranging for  $q$  gives us:

$$q = \pi L \kappa \cdot \frac{T_1 - T_2}{\ln\left(\frac{r_2}{r_1}\right)} \quad (4)$$

Combining the results with the equation for  $\Delta T$  finally gives us an expression for the thermal resistance through the fluid:

$$R_{th,f} = \frac{\ln\left(\frac{r_2}{r_1}\right)}{\pi L \kappa} \quad (5)$$

The variables in equation (5) are approximated in order to make an estimation of the magnitude range of the resistance. Firstly, the thermal conductivity of the measured liquids lies between 0.168 (isopropanol) and 0.617 (water)

[W/mK]. The calculation of the radii is rather straightforward the inner radius is 5.5 [ $\mu\text{m}$ ] following from the heater's width of 11 [ $\mu\text{m}$ ]. The distance between the heater and the substrate is designed to be 20 [ $\mu\text{m}$ ], hence it follows that the outer radius has a value of 25.5 [ $\mu\text{m}$ ]. Lastly, the length of the channel is 1.0 [mm]. Together these parameters give the thermal resistance a value in the range of 790 and 2900 [K/W]. The second thermal resistance consisting of the heat conduction to the substrate through the channel walls ( $R_{th,w}$ ) is approximated by a slab-like geometry. The resistance is influenced by the length of the channel, the thickness of the SiRN walls, and the distance between the heater and the substrate. The walls are present equally on both sides of the channel. Hence the calculated resistance can be halved, as the two equal resistances are in parallel. The final expression describing  $R_{th,w}$  is given by:

$$R_{th,w} = \frac{1}{2} \cdot \frac{d}{W \cdot L} \cdot \frac{1}{k} = 8.8 \cdot 10^3 - 1.8 \cdot 10^4 [\text{K/W}] \quad (6)$$

The value of the thermal resistance through the walls is approximated using the thermal conductivity of low-pressure chemical vapor deposition (LPCVD) SiRN, 3.5 [W/mK] [5] in combination with the dimensions found in table 1. The last thermal resistance consists of the heat conduction within the substrate combined with the heat convection to the air. The thermal conductivity of silicon is roughly 140 [W/mK] depending on the source, this makes the share of the thermal resistance attributed to the thermal conduction within the substrate insignificant. However, the amount of heat convection is hard to approximate due to the intricate packaging surrounding the chip. Therefore, the size of  $R_{th,s}$  is based on empirical findings. Together these resistances make the analogous circuit that can be seen in figure 2.

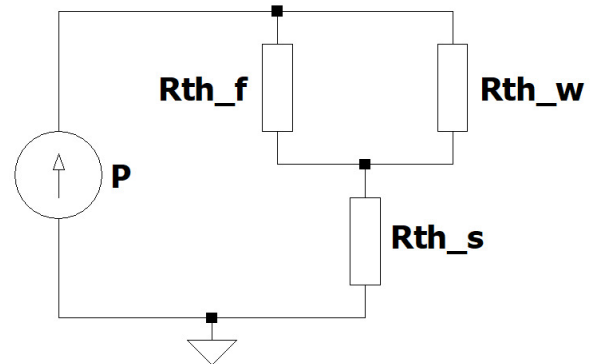


Figure 2: Circuit equivalent model

### 3D MODELING

The thermal circuit model neglects a few effects that do in reality affect the thermal behavior within the sensor, e.g. the flow velocity. In industry, it is customary to simulate MEMS devices using Finite Element Modeling (FEM) software to justify design choices before fabrication takes place. This is the reason for 3D FEM analysis (COMSOL)

in the analysis of the thermal conductivity sensor. The sensor overview in figure 1 is too detailed to be used as the geometry for the purpose of FEM analysis. The model is simplified for the sake of computational intensity and meshing quality. A cross-section of the simplified model can be seen in figure 3. The components are the same as in the detailed overview. A few notable changes have been made to simplify the model: the channel is made strictly rectangular. Furthermore, the silicon bulk has been reduced to a mere contact point with a constant temperature forced at the external boundaries, i.e. an infinite heat sink, to simulate a larger entity. Lastly, an air box has been added that surrounds the channel on all sides. Again, having a constant temperature at the outer boundaries for the sake of virtually creating a larger entity that can store more heat, like a real room filled with air could. These boundary conditions eliminate the need for life-size modeling of such environments that would complicate the model beyond a reasonable amount. The boundaries that have a constant temperature assigned are marked in red. These simplifications become significant when one starts meshing the structure, i.e. dividing the structure into small elements. The characteristics of these elements will then be individually evaluated based on the chosen multi-physics. The simulation can be used to provide further insight into the effects that certain parameters can have on the system. For example, adjusting mass flow in sweeps can help gauge the flow-dependency of the sensor.

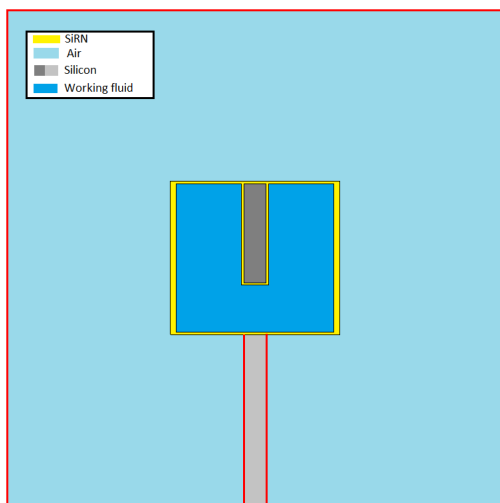


Figure 3: Simplified model of the thermal conductivity sensor.

The data that is most relevant, is the temperature of the fluid vertically adjacent to the location of the platinum readout track. The sensing track spans the entire length of the chip. It exhibits a temperature that consists of the average temperature in the fluid below it due to the high thermal conductivity of metals. To estimate the temperature rise recorded in reality it is best to plot the calculated temperature against the position in the channel along the direction of flow. The first test case to assess the validity of the model is to step-

wise increase the heat applied by the heater. A linear relation between applied heat and temperature rise is to be expected. In figure 4 one can observe the temperature profile of the fluid right under the platinum temperature sensor with a mass flow of 1 [g/h]. There are three main conclusions to draw from this figure. Firstly, both endpoints of the channel experience ambient temperature, which is intentional since the liquid is surrounded by the highly heat-conductive substrate from those points onwards.

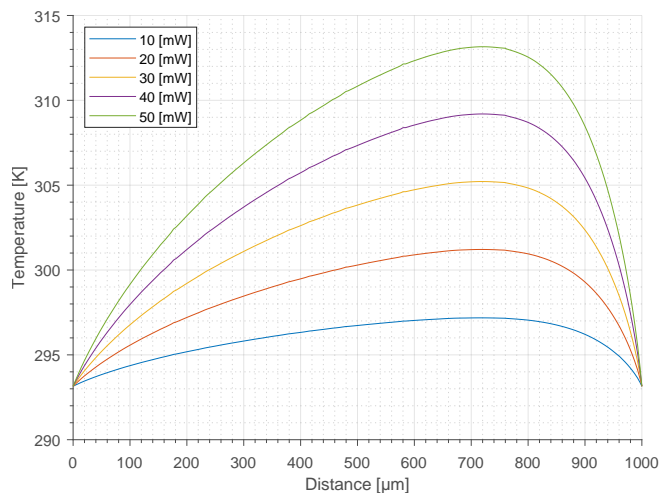


Figure 4: Simulated temperature at the location of the readout sensor along the channel length for a variety of heat rates.

Furthermore, the flow impacts the temperature profile in such a way that it shifts the maximum temperature point further towards the outlet. In situations unaffected by flow one would expect the maximum temperature exactly in the middle of the boundary conditions. Lastly, the temperature rise appears to scale linearly with the applied heat rate. Confirmation is shown in figure 5, where the average temperature increase of each respective curve is plotted against the respective heat rate used.

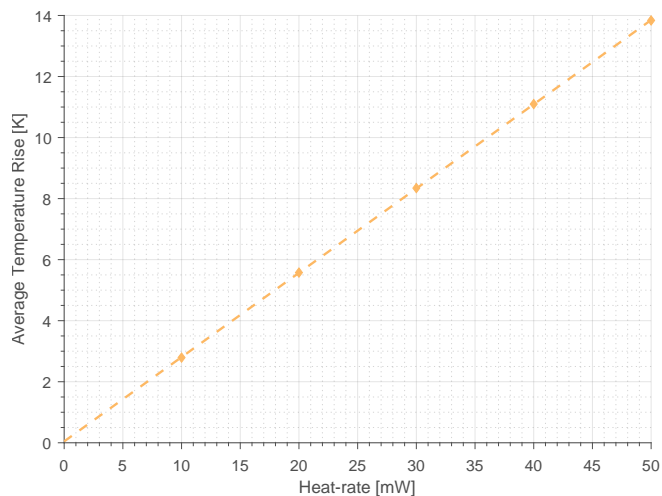


Figure 5: Verification of linearity regarding applied heat rate

The mass flow rate significantly affects the thermodynamics within the sensor as has become evident from the previously acquired data. Therefore, a second parameter sweep aims to illustrate the precise effect that mass flow rate has on the relevant temperature profile. The rate at which the working fluid passes the heater does not only alter the temperature profile, it also affects the induced temperature rise due to lateral heat conduction by means of flow as can be seen in figure 6. Consequently, a lower mass flow leads to a higher resolution in the form of increased temperature rise and greater accuracy as it limits the heat conduction through flow. In addition to the specified 1 [g/h] mass flow, the final characterization is carried out under no flow conditions due to the evident influence of flow. This way the temperature rise is mostly governed by thermal conductivity.

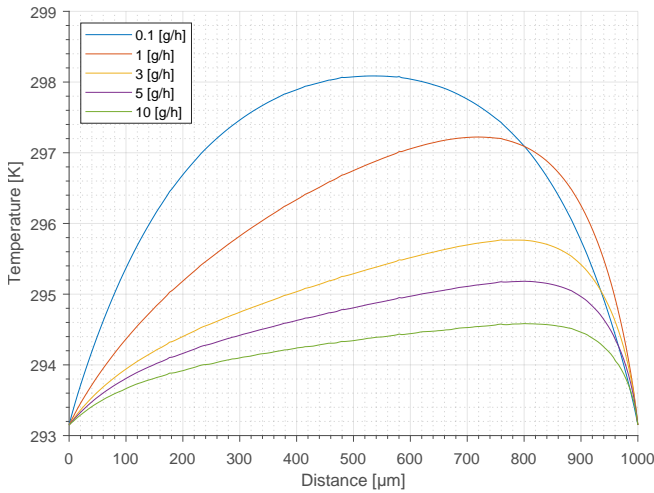


Figure 6: Simulated temperature at the location of the readout sensor along the channel length for a variety of mass flow rates.

During fabrication, the silicon bulk adjacent to both sides of the channel has been etched to thermally isolate the channel and therefore increase its sensitivity. However, the size of the contact with the bulk or even the existence of said contact is rather uncertain. Geometric sweeps have been analyzed to gauge the influence of the contact size together with the consequences of total disconnection from the bulk. In figure 7 we can see that a significant increase in contact area has an effect on the recorded temperature rise, albeit rather small.

More significantly, any amount of separation from the bulk leads to a drastic increase in temperature as seen in figure 8. This can be attributed to the additional thermal resistance imposed by the gap of air. The total thermal resistance is greatly increased due to air having a rather low thermal conductivity of 0.025 [W/mK]. Connection to the substrate is paramount for the sensor as an existing air gap introduces a large additional series resistance. The additional thermal resistance reduces the influence that the working fluid's thermal conductivity has on the total thermal resistivity. Which in turn reduces the distinction in temperature rise between liq-

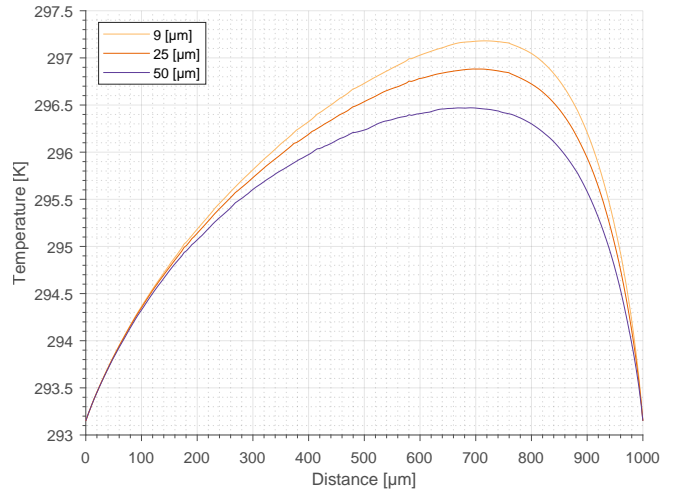


Figure 7: Simulated temperature at the location of the readout sensor along the channel length for a variety of contact widths

uids of varying thermal conductivity, consequently lowering the sensor's sensitivity.

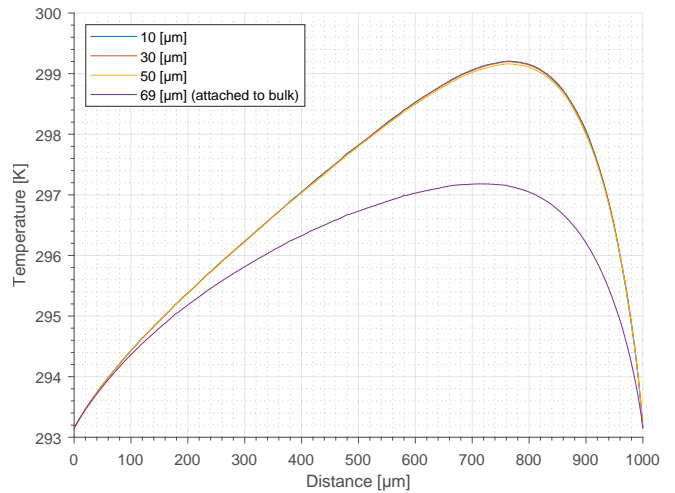


Figure 8: Simulated temperature at the location of the readout sensor along the channel length, consequences of separation between channel and bulk.

Finally, we investigate the influence that the working fluid has on the perceived temperature profile by performing simulations on ethanol, ethylene glycol, glycerol, and water. These fluids have a thermal conductivity in ascending order of 0.169, 0.201, 0.292, and 0.617 [W/mK] respectively [6]. The goal of the simulation is to verify that the sensor can distinguish the liquids based on thermal conductivity. To eliminate any contribution from the flow it was simulated at near no flow conditions (0.01 [g/h]). Furthermore, it must be noted that the standard geometry depicted in figure 3 was utilized for the simulation. There is a distinction in temperature rise between the liquids as can be seen in figure 9. These results gained from the simulation are compared with empirical data in a later section to assess the model's accuracy.

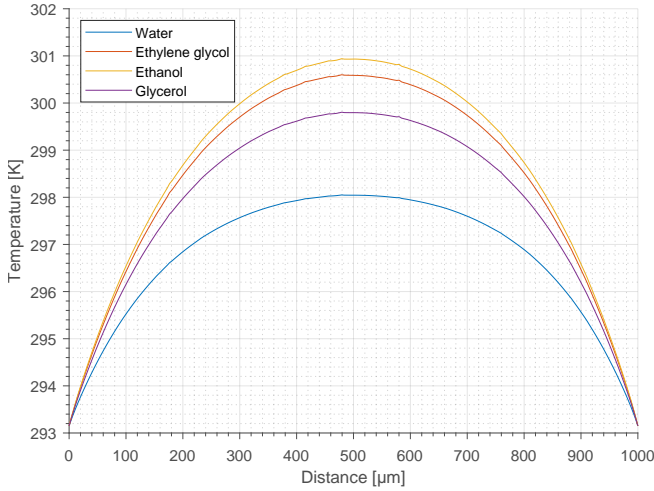


Figure 9: Simulated temperature at the location of the readout sensor along the channel length for a variety of liquids.

## HEAT TRANSFER

An observation about the non-uniform magnitude of the temperature profile throughout the channel is based on the acquired temperature plots. Ideally, one would like the temperature to rise to a certain maximum temperature quickly. In addition, it should remain constant throughout the length of the channel. This makes sure that one can obtain an accurate temperature measurement which is dominated by the thermal conductivity of the working fluid. A temperature distribution with a parabolic shape indicates that lateral heat transfer to the in and outlet boundaries are of larger magnitude than the heat transfer between the heater and bulk through the working fluid. The shape of the temperature distribution is governed by the following relation [7]:

$$\Delta T(y_n) = \frac{P'}{G'_f} \left( 1 - \frac{\cosh\left(y_n \cdot l \sqrt{R'_b G'_f}\right)}{\cosh\left(\frac{1}{2}l \sqrt{R'_b G'_f}\right)} \right) \quad (7)$$

Where  $\Delta T$  represents the temperature as a function normalized from -0.5 to 0.5 of the channel length where 0 represents the center of the channel. The variable  $P'$  represents the line power in [W/m],  $G'_f$  is the thermal line conductance of the working fluid adjacent to the heater, similarly  $R'_b$  represents the thermal line resistance of the structure in [W/K·m], lastly  $l$  signifies the length of the channel. The solution above represents the temperature distribution. It is plotted for a variety of channel lengths. The flattening of the temperature profile is influenced quadratically by channel length and linearly by the magnitude of the line resistance and conductivity [7]. The result depicted in figure 10 shows that using the current geometry, the channel needs to be at least 5 mm and preferably 10 mm long to exhibit a reasonably flat temperature profile away from the boundary conditions. A constant temperature throughout the channel's length ensures that the thermal conductivity of the working fluid governs the extent of the maximum temperature for the most part,

i.e. diminishing the effect of lateral heat flow.

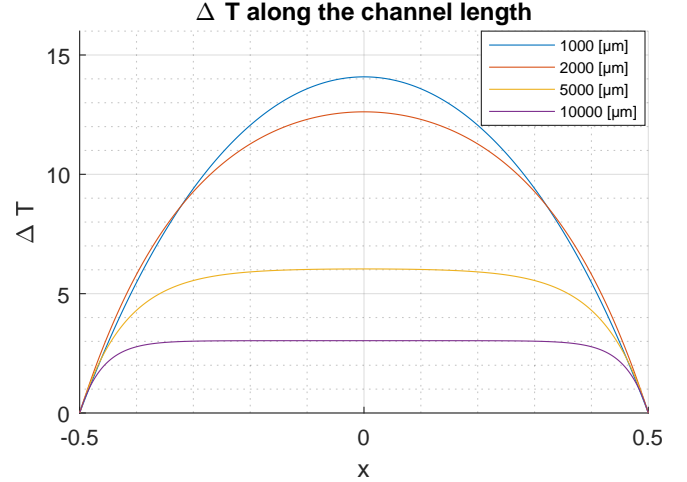


Figure 10: Equation (7) visualized with a variety of channel lengths.

A simulation in COMSOL was run sweeping over a variety of channel lengths to further reinforce the validity of the theory. The temperature profiles acquired by means of simulation are depicted in figure 11. These profiles show a clear resemblance to the profiles gained from theory. A slight difference is the asymmetric appearance of the distributions. The asymmetry can be attributed to the effect that 1 g/h mass flow has on the temperature profile. Furthermore, a decrease in temperature rise can be observed as the channel length increases. The cause is that an increase in channel length enlarges the conductive area as well as the internal volume of the heater. Meaning that the heat has a larger volume to spread over, thus reducing temperature rise.

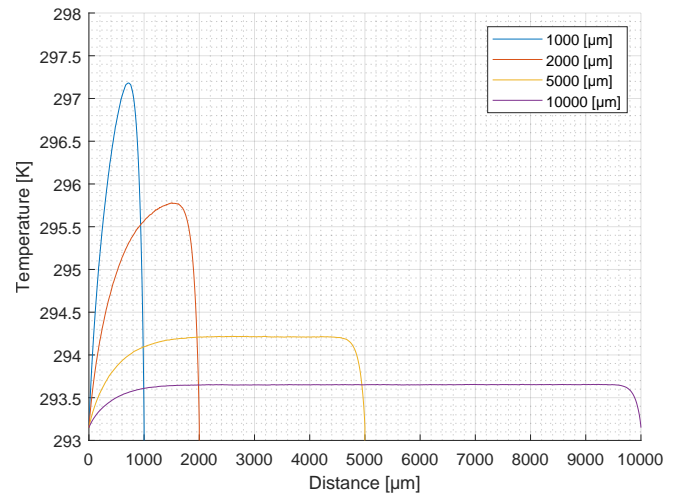


Figure 11: Simulation of the temperature profile plotted along the channel length for a variety of channel lengths.

## METHOD & RESULTS

As previously mentioned, the main goal of the research is the characterization of the thermal conductivity sensor. A fitted line constructed by measurements performed on a variety of fluids with differing thermal properties is essential to the characterization of the thermal conductivity sensor. To ensure a steady state response independent of heat capacity the data will be gathered under no flow conditions in addition to the standard 1 [g/h] mass flow. The fitted line contains information about the relation between a rise in temperature and thermal conductivity. The slope of the fitted line together with the offset can be utilized to enable the calculation of thermal conductivity based on the measured temperature/resistance rise, i.e. characterize the sensor.

### Test Setup

The block diagram in figure 12 shows a schematic overview of the test setup that was used to extract the data required to characterize the thermal conductivity sensor. A nitrogen tap provides the required pressure to drive the fluid through the setup. It is followed by a pressure controller that is used to manually set an amount of pressure to prevent any damage to the chip and other components. The pressure controller is then connected to a flask that holds the working fluid going into the chip. However, before going into the chip it passes two components that are vital to the setup. Firstly, it passes the Flow-lab multiple times through interconnected loops. This device makes sure that no gasses remain in the fluid to help prevent air bubbles from manifesting inside the microfluidic channels of the chip. Before entering the chip it passes a mass flow controller as the readings are flow dependent. A power supply with the capability of measuring its supplied power is used to provide accurate DC excitation to the heater. The digital multimeter measures the resistance of the readout track before every measurement to calibrate the idle resistance of the sensor. The multimeter records the change in resistance as the current is supplied to the heater. The increase in resistance is recorded when the system is in steady-state, i.e. when the resistance settles after a few seconds of excitation. The equation in figure 12 is then used to convert this change in resistance into an actual rise in temperature. This equation requires  $\alpha$ , the TCR of platinum. This value was measured to be 0.002717 during earlier research.

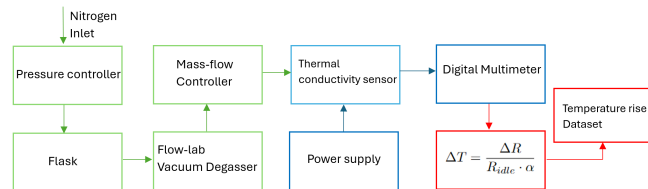


Figure 12: Block diagram of the test setup, fluidic components in green, electrical in blue, and mathematical in red.

### Influences of mass flow and heat rate

A couple of tests are carried out with water as the working fluid before characterizing the sensor by extracting the fitting coefficient. The goal of these tests is to gauge the influence of mass flow and heat rate. These tests are performed under the same conditions as the simulation. This allows for a correct comparison between the two. The first validating test proves the hypothesis of linearity between applied heat and temperature rise. The application of a series of incremented voltages is used to force an increasing heat rate onto the sensor. A secondary aim is to gain insight into what magnitude of heat rate is large enough to ensure a decent resolution while making sure that the induced temperature rise remains lower than 10 [K] for the entire range 0.15-0.7 [W/mK]. An excessive temperature rise could induce chemical reactions that have adverse effects on the sensor's accuracy. The test was carried out at a mass flow of 1 [g/h], i.e. the mass flow that the sensor was designed for to match results from the simulation. The results of the voltage sweep in comparison to the simulated data can be found in figure 13. It must be noted that only two data points are required to sketch the graph for the simulated data due to the perfect linearity shown in figure 5. The findings confirm that in reality the temperature rise is indeed linearly dependent on the applied heat rate. It also gives an indication of the correct voltage to apply for the final characterization of the sensor. Keeping in mind that the thermal conductivity of water resides at the very high end of the sensors range.

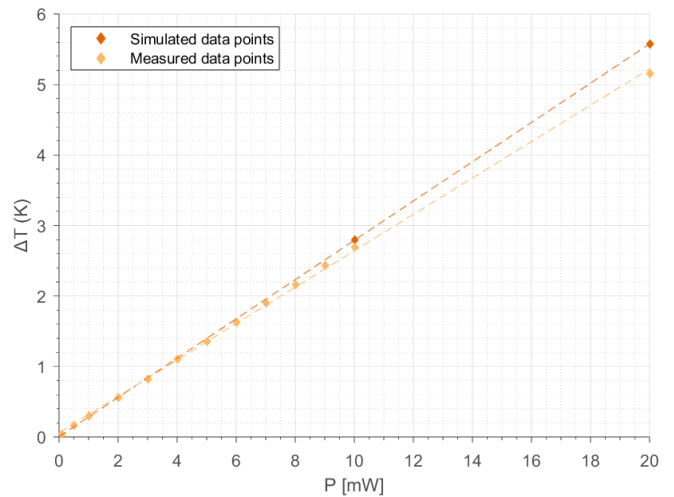


Figure 13: Simulation versus Measurements, comparison of the influence of heat rate.

Secondly, we establish the effect that mass flow has on the temperature readings using the mass flow controller to regulate the flow. From figure 14 we conclude that the effect that flow has on the sensor proves less severe in reality. However, to accurately assess thermal conductivity a mass flow controller still seems to be needed.

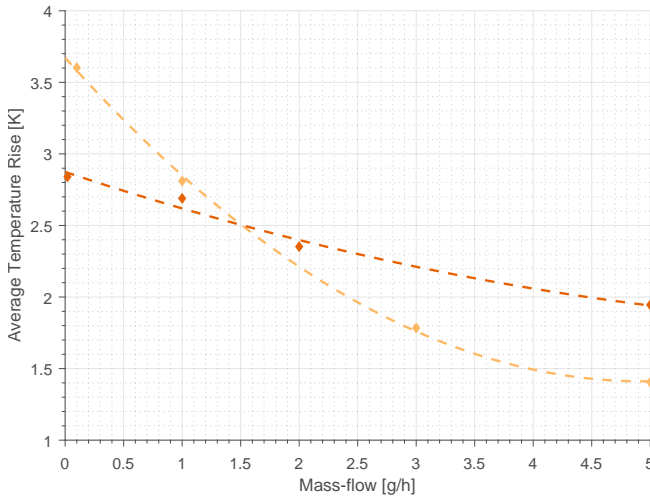


Figure 14: Simulation versus measurements, comparison of the influence of mass-flow using a 10 mW DC excitation

### Characterization

To use the sensor properly, one needs to know what temperature corresponds to the correct thermal conductivity. The thermal conductivity of most available liquids lies close together between 0.15 and 0.25 [W/mK], with water having a thermal conductivity of 0.617 [W/mK]. Water and ethanol were mixed in different weight percentages to obtain a dataset ranging from 0.168 to 0.617 [W/mK] with roughly equal spacing in thermal conductivity between measurements. These data points were used to create a line-fitted polynomial. The coefficients associated with said polynomial can be used to translate temperature into thermal conductivity. From the theory in the analysis section, we know that thermal conductivity affects the temperature rise in an inversely proportional manner. Therefore, it results in a  $1/x$  shaped graph when plotting temperature rise on the  $y$ -axis against thermal conductivity on the  $x$ -axis. Whilst gathering data, we encountered inconsistent measurements regarding the amount of temperature rise associated with a liquid. The difference is upwards of a factor 2.5 under no flow circumstances. Possible causes for the inconsistent measurements will be discussed in the following section. In figure 15 we see the measured temperature rise against the known thermal conductivity found in [6]. The measurements lie within a 2% full scale error from the fitted line. An additional 5% error margin has been attributed to the known thermal conductivities due to the measurement uncertainty mentioned in [6]. Note that the data was gathered under no flow conditions and that the percentages indicate a weight percentage of ethanol in water.

Table 2: Characterization coefficients

Polynomial degree	zero	first	second
Coefficients (k-method)	10.0762	-18.4880	11.1765
Coefficients (1/k-method)	1.7881	0.9767	

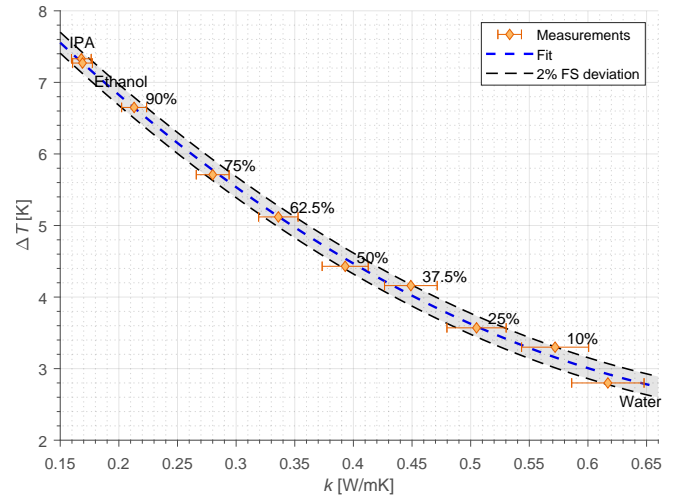


Figure 15: Characterization of the thermal conductivity sensor with a second order polynomial under no-flow conditions, within 2% of the full scale (FS) deviation.

Another option is to plot the temperature rise against the reciprocal of the thermal conductivity. The relationship between these should in theory be linear since the temperature rise is inversely proportional to the thermal conductivity. From figure 16 one can see that the relation is not strictly linear. Possible reasons for these deviations are discussed in the next section. These deviations cause a larger error (8% full scale). The characterization coefficients stemming from these plots can be found in table 2.

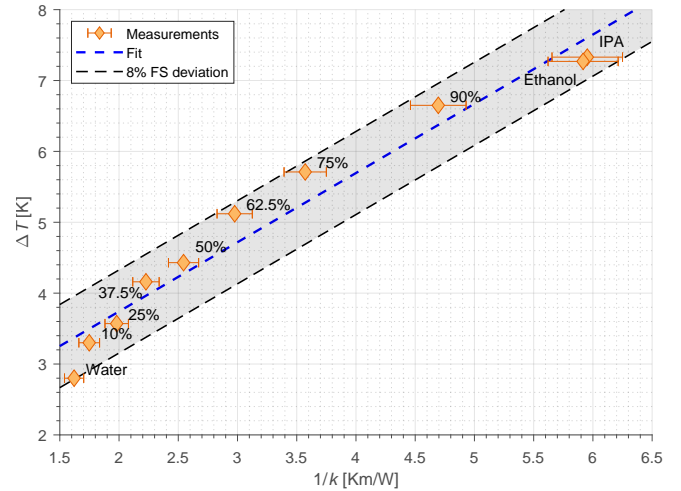


Figure 16: Characterization of the thermal conductivity sensor with a first-order polynomial.

One can refer to appendix section B for similar plots created from a dataset gathered with a mass flow of 1 [g/h], these plots prove that the device can be used under non-zero flow conditions.

To see how well the measurements follow both theory and simulation, we compare the measurements against both theory and simulation. The comparison is done under no flow

conditions to have a fair verdict on the likeness between theory and reality. A couple of corrections are made to achieve likeness between theory and measurements. A correction coefficient of 0.22 was applied to the fluid's thermal resistance. In addition, the substrate's thermal resistance with the surrounding air was determined to be 160 [K/W]. These corrections can be justified as the theoretical heat flow was simplified into a one-dimensional problem to make it calculable. The resulting graph is shown in figure 17.

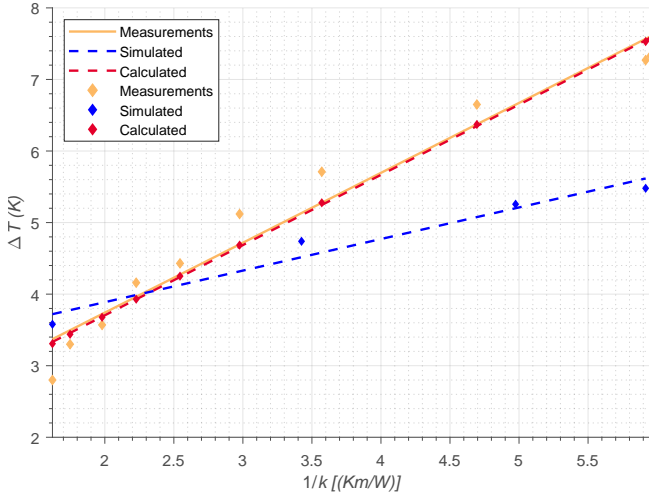


Figure 17: Characterization comparison between calculation, simulation, and reality

## DISCUSSION

There are a few notable findings to discuss. Firstly, measurements proved to be inconsistent. Several reasons that could possibly explain these inconsistencies are investigated. Firstly, the temperature change in the substrate was monitored. The reason being that a relatively hot substrate does not conduct the heat from the channel as well and therefore influences measurements. Through the use of the reference sensor, it became clear that the substrate did not heat up significantly due to long-term exposure to heat supplied by the DC excitation of the sensor's heater. The temperature change fluctuated slightly as can be seen in appendix section C. The fluctuation shown is more likely than not to be caused by a change in room temperature. Another observation made during measurements was the fact the temperature change measured seemed to slowly decline. After the insertion of a working fluid, the temperature change took a long while to settle to a final value. A multiple-hour-long experiment was carried out, to ensure that the temperature did indeed settle and not fluctuate. The graph in appendix section C shows that the temperature change did indeed settle and can therefore not be credited for the discrepancies. These findings make it highly likely that the issue lies within the fluid domain of the sensor. Preventing the formation of air bubbles within the microchannels is a large challenge in microfluidics [8] and could possibly be the source of the experienced inconsistencies and discrepancies. The presence of air bubbles in

critical positions lowers the magnitude of thermal conductivity locally. Overall thermal resistance will rise as a result, inducing a larger temperature rise associated with the same fluid. These inconsistencies occurred when flushing the chip dry with nitrogen. According to [8] pre-filling the device with a low surface tension liquid can help alleviate these issues, a precaution that was unintentionally taken for measurements displayed in the previous section. However, further research is required to pinpoint the cause for these inconsistent findings with more certainty. Lastly, there is the fact that the thermal resistance calculated from the one-dimensional model requires a correction coefficient of 0.22. The geometry used in the model varies substantially from reality due to simplifications. Furthermore, a large portion of the heater's surface area was neglected in the model. The fluid directly between the heater and the substrate was the only medium of heat transfer to be considered. In reality, it is much larger in volume. All these simplifications cause the thermal resistance to appear greater than it is and therefore a correction coefficient between zero and one is to be expected.

## CONCLUSION

A first attempt has been made to characterize the thermal conductivity sensor. The paper provides two fitting coefficients that can be used to ascertain the thermal conductivity of the analyzed liquid based on the measured change in resistance. Results show that the accuracy of thermal conductivity sensing lies between 2 and 8 percent of the full scale, depending on the chosen characterization method. Furthermore, the sensor can be used with a known mass flow as long as it is acknowledged and compensated for. The channel of the sensor could be made longer to obtain a more constant temperature profile. Efficiency can be improved upon by discovering what causes the long settling time, another option is to compensate for it effectively. Lastly, further research is required into the cause of the sensors' inconsistency. Solving these difficulties may help towards a future where liquids can be characterized quickly and efficiently.

## References

- [1] Ángel Ríos, M. Zougagh, and M. Avila, “Miniaturization through lab-on-a-chip: Utopia or reality for routine laboratories? a review,” *Analytica Chimica Acta*, vol. 740, pp. 1–11, 2012.
- [2] J. Groenesteijn, M. J. DeBoer, J. C. Lötters, and R. J. Wiegink, “A versatile technology platform for microfluidic handling systems, part i: fabrication and functionalization,” *Microfluidics and Nanofluidics*, vol. 21, 2017.
- [3] M. E. O’Hagan, “Measurements of the thermal conductivity and electrical resistivity of platinum from 100 to 900c,” *Journal of research of the National Bureau of Standards - C. Engineering and Instrumentation Vol. 71C, No. 4*, 1967.
- [4] R. S. Subramanian, “Conduction in the cylindrical geometry,” tech. rep., Department of Chemical and Biomolecular Engineering, Clarkson University.
- [5] H. Ftouni, C. Blanc, D. Tainoff, A. D. Fefferman, M. Defoort, K. J. Lulla, J. Richard, E. Collin, and O. Bourgeois, “Thermal conductivity of silicon nitride membranes is not sensitive to stress,” *Phys. Rev. B*, vol. 92, p. 125439, Sep 2015.
- [6] Fluidat On The Net, Database by Bronkhorst containing physical properties of liquids and gasses.
- [7] J. van Baar, *Distributed thermal micro sensors for fluid flow*. PhD thesis, University of Twente, 2002.
- [8] X. Zhao, C. Ma, D. S. Park, S. A. Soper, and M. C. Murphy, “Air bubble removal: Wettability contrast enabled microfluidic interconnects,” *Sensors and actuators. B, Chemical*, 2022.

# Appendices

## A Declarations

During the preparation of this work the author used the chatbot ChatGPT based on GPT-3.5 to aid in the process of converting raw data into legible plots. Furthermore, Grammarly was used to spot spelling and slight grammatical errors after the thesis was written in full.

## B Additional characterization plots (1 g/h)

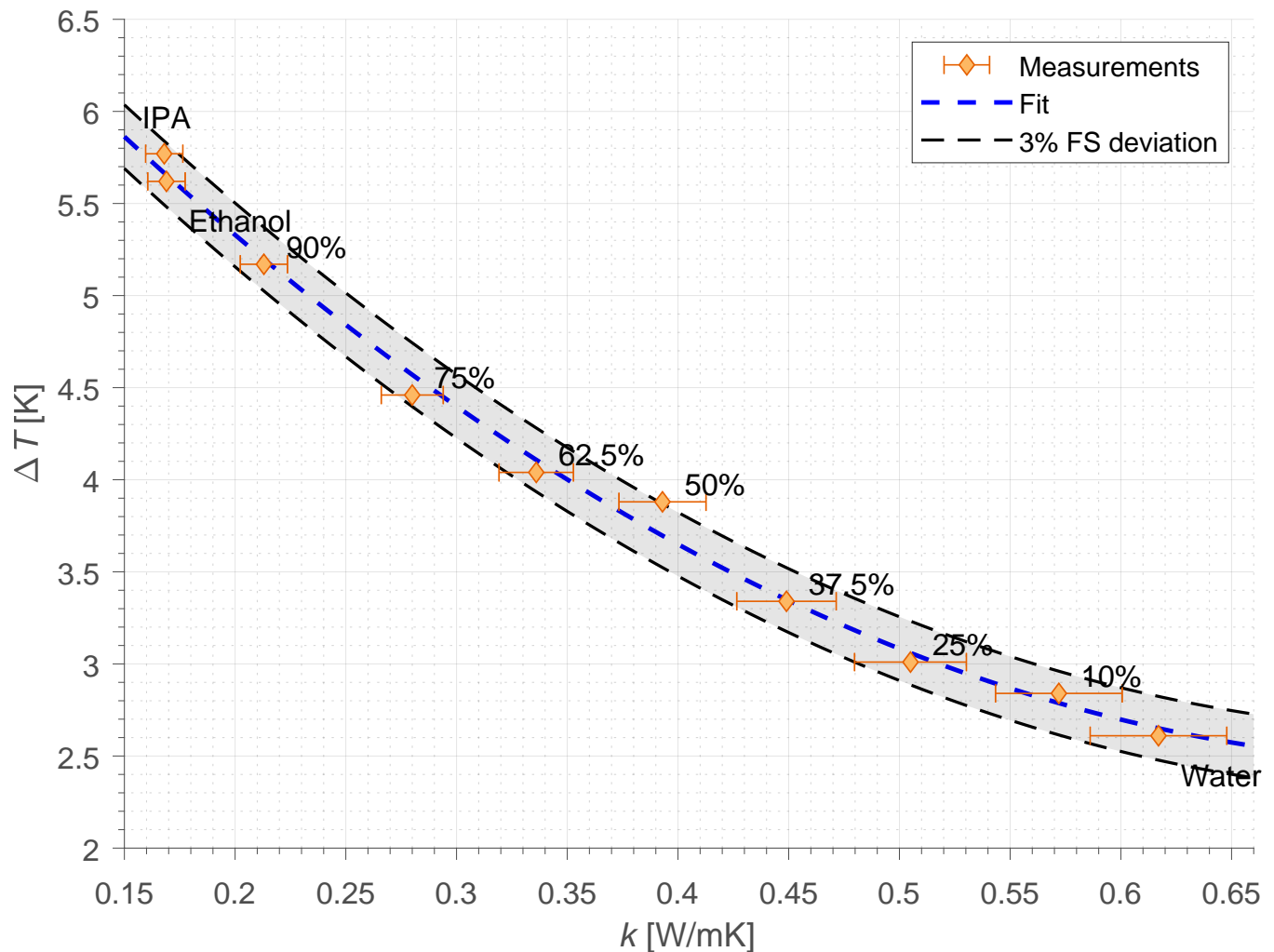


Figure 18: Characterization of the thermal conductivity sensor with a second order polynomial under 1 g/h mass flow conditions, within 3% of the full scale (FS) deviation.

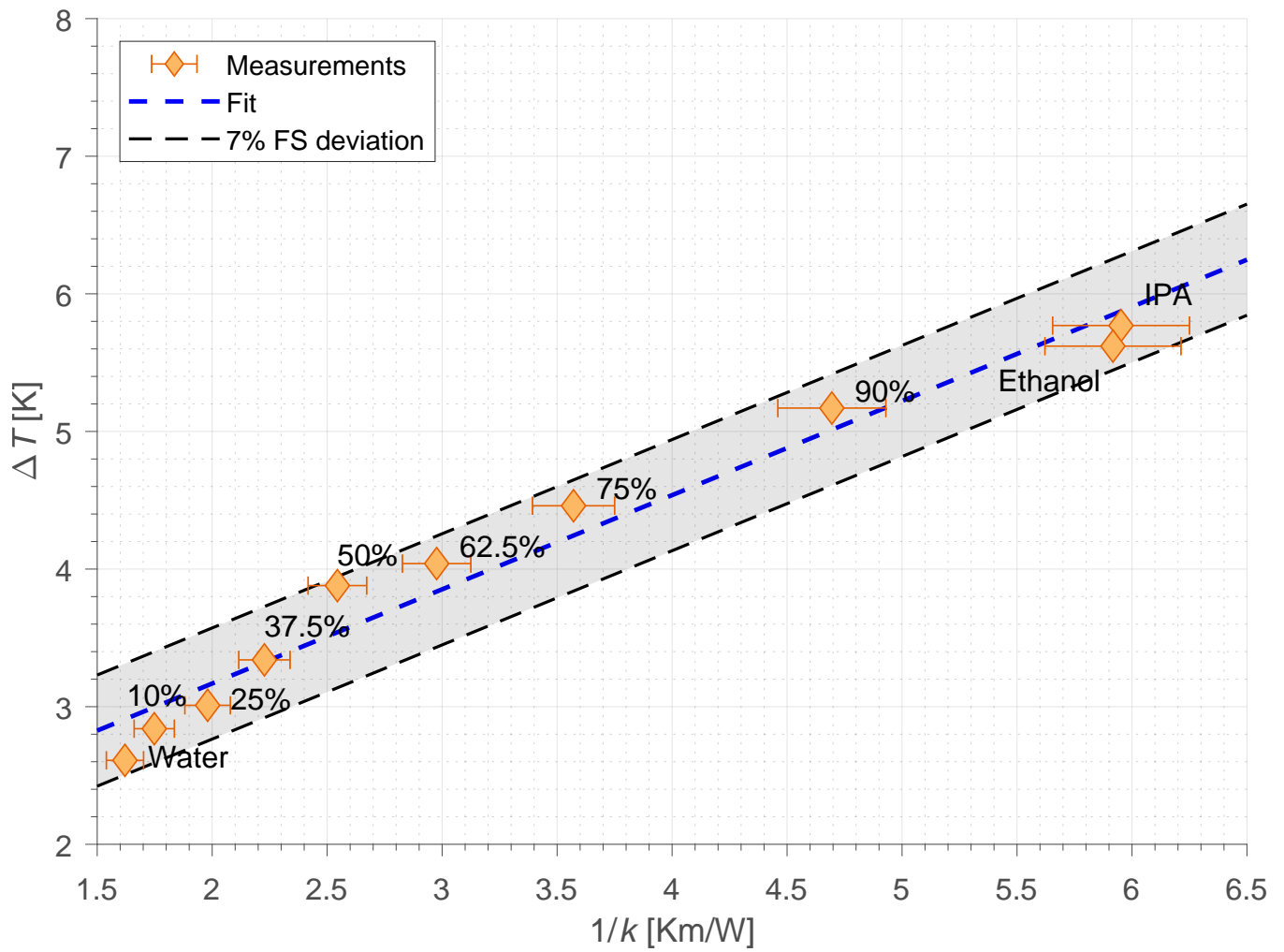


Figure 19: Characterization of the thermal conductivity sensor with a first order polynomial. Carried out under 1 g/h mass flow.

## C Validation

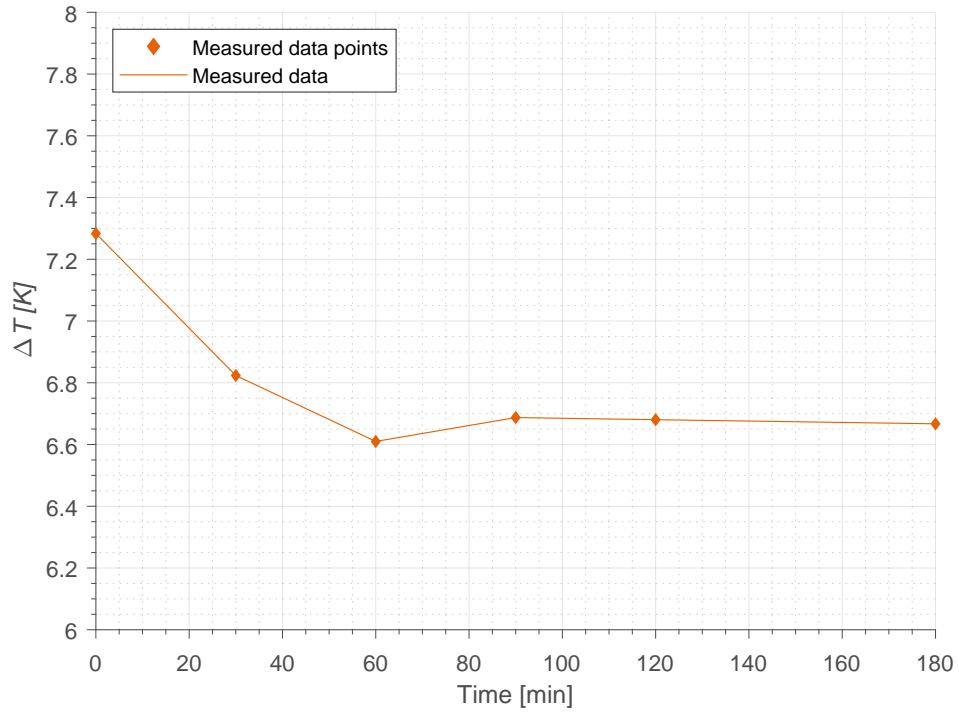


Figure 20: Periodic measurements of temperature rise to validate that the temperature indeed settles and does not fluctuate by a significant amount

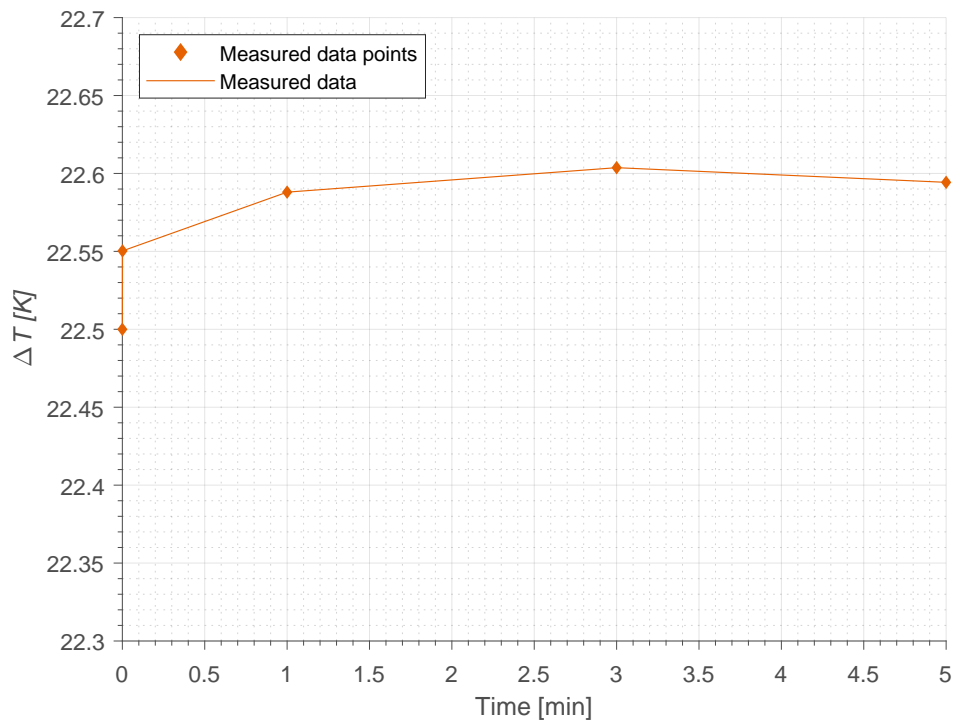


Figure 21: Periodic measurements of temperature rise to validate that the substrate does not heat up drastically during the usual measurement time of around 1 minute.